Coarse-Grained Simulation of Polycation/DNA-Like Complexes: Role of Neutral Block

Bicai Zhan,[†] Kaihang Shi,[†] Zhexi Dong,[†] Wenjie Lv,[§] Shuangliang Zhao,*[,†] Xia Han,*[,‡] Hualin Wang,[§] and Honglai Liu[†]

[†]State Key Laboratory of Chemical Engineering, [‡]Department of Chemistry, and [§]State Environmental Protection Key Laboratory of Environmental Risk Assessment and Control on Chemical Process, East China University of Science and Technology, Shanghai 200237, China

S *Supporting Information*

ABSTRACT: Complexes formed by polycations and DNA are of great research interest because of their prospective application in gene therapy. Whereas the applications of multiblock based polycation generally exhibit promising features, a thorough understanding on the effect of neutral block incorporated in polycation is still lacking. By using coarse-grained dynamics simulation with the help of a simple model for solvent mediated interaction, we perform a theoretical study on the physicochemical properties of various polyplexes composed of a single DNA-like polyanion chain and numbers of linear polycationic chains with different modifications. By analyzing various properties, we find the hydrophobic/hydrophilic modifications of linear polycations may bring an improvement on one aspect of the properties as gene carrier but also involve a trade-off with another one. In particular, polycation with a hydrophobic middle block and a hydrophilic tail block display distinct advantages among di- and triblock linear polycations as gene carrier, while careful design of the hydrophobic block should be made to reduce the zeta potential. The simulation results are compared with available experimental data displaying good agreements.

KEYWORDS: *triblock, polycation, gene carrier, simulation, polymer*
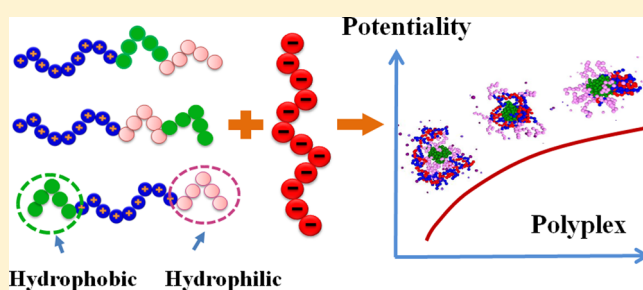
1. INTRODUCTION

Gene therapy has been regarded as a promising and ultimate cure for many life-threatening diseases, acquired or inherited, such as AIDS, cancer, and genetic disorders.[1] A persistent challenge in transforming this idea of gene therapy into clinical medicine is the safe and effective delivery of therapeutic genes in vivo to targeted cells. Toward this goal, numerous efforts have been devoted to the design and optimization of efficient delivery vehicles.[2−5] Because drug molecules are usually negatively charged with molecular weights on the order of 10^6 for a gene to 10^3 for an oligonucleotide, a successful delivery vehicle should primarily overcome the passive diffusion of drug molecules crossing cell membranes.[6,7] The resistance originates physically from the electrostatic repulsion, and this generally requires the carrier to be positively charged and thereafter can eliminate the repulsion between the delivery system and cell membranes.[8] Second, the volume of delivery system is supposed to be as compact as possible so as to reduce the exclusion during the endocytosis.[2,9] Lastly, the delivery vehicle should be desired to protect DNA from being degraded by nucleases, which are present in normal plasma, and this demands the carrier can closely pack up the DNA inside.[2,3]

A vast majority of gene delivery is initially attempted using viruses as gene carriers because virus vectors are efficient in carrying foreign genes into cells.[5,10] However, the toxicity and immunogenicity of virus vectors greatly limit their clinical applications.[11] Liposome and shelled nanoparticles are also substantially investigated as gene carrier, and progress has been made along this direction.[3,12] In recent decades, much attention has been shifted to various polycations for their encouraging merits such as easy structure modification, capability to carry large inserts and facile manufacturing.[2,3] Polycations including polyethylenimine (PEI),[13,14] polylysine (PLL),[15] poly-(amidoamine) (PAMAM) dendrimers,[16,17] and poly(2-(dimethylamino) ethyl methacrylate) (PDMAEMA)[17,18] are capable of condensing negatively charged DNA into stable nanosized particles.

While simple homopolymer-based polyplex formulations have proven to be very effective in vitro gene transfers, they are unsuitable for in vivo applications because they can be rapidly cleared from the circulation.[13] Recently, it has been reported that the delivery system coated with bioinert water-compatible polymers can give rise to a steric stabilization of the delivery vehicle against undesirable aggregation and nonspecific electrostatic interactions with its surroundings.[19−23]

It has been found that water-compatible neutral blocks incorporated in polycations impose strong influence on the morphology of polyplex and thereafter affect the biological activity of the complex.[3,20−24] The polycations containing one or more additional neutral blocks present promising performances of the polyplexes at various aspects including cellular uptake, endosomal escape, and timely release of the encapsulated DNA.[17,25−27] Whereas the applications of multi-block copolymers generally exhibit promising features toward targetable and endosome disruptive nonviral gene vectors,[25−27] opposite effects are also found.[17,27] Sharma et al.[17] reported that micelleplexes composed of triblock copolymers, i.e., polycation with one hydrophilic block at the other end and one hydrophobic block in the middle, were not better than the corresponding homopolymer-based polyplexes in terms of both prevention of PAA-induced dissociation of polyplex and protection of the encapsulated DNA. The ostensible controversy is essentially concerned with the interpretation of the roles of neutral block in polycation for gene delivery.

The purpose of present work tends to address the effects of neutral block incorporated in polycation on the formulations of polycation/DNA-like complex by using computer simulation. Computer simulation can simplify the experimental detail, yet probe into the nature of problems and provide guidelines on how to tune the polycation architecture, and this helps finally to engineer proper copolymers as gene carriers. By means of simulation, the effects of chain length, architecture, stiffness, concentration of counterion, charge valence, and the strength of electrostatic interaction on the formulations of polyplex have been investigated.[28−33] Those simulation works could supply atomistic details for polycation−DNA binding, e.g., DNA binding with PLL,[34] PEI,[31,33] or with poly(amidoamine) (PAMAM) dendrimers,[35] and provide coarse-grained yet full-sized pictures for the formulation processes of poly-plexes.[29,32,36−40] For instances with coarse-grained simulations, Stevens[30,38,41] found that the condensation of a single polyelectrolyte chain in the presence of trivalent and tetravalent counterions led to a complex with the morphology of toroid or rod depending on the stiffness of the polymer, and Ziebarth[28] showed that an increase in the block length of cationic or neutral block in copolymer drove the structure of the complex more closely to the so-called core−corona morphology. All those excellent simulation works cast helpful insights toward an improved understanding of the formulations and transfections of various polyplexes.

In this work, coarse-grained simulation method is adopted to investigate the effects of hydrophobic/hydrophilic block of polycations on the formation and morphology of entire complex. The DNA-like chain is modeled with a negatively charged linear homopolymer, and the polycations considered here are linear block copolymers incorporated with hydro-phobic or/and hydrophilic block(s). Although this model is far from accurate to describe the molecular details of a DNA chain, it captures the major characters of DNA-like chain and thus provides a good testing model to address the above-mentioned problem. Similar to previous work,[29,37] here we consider only one polyanion chain contained in the simulation system for simplification, which, in practice, corresponds to a dilute DNA solution. By accessing the radial distribution, square radius of gyration, aggregation number, etc., we make comparisons for the polyplexes composed of various kinds of polycations on the aspects of size, water solubility, packing degree, zeta potential,

etc., and thereafter analyze the defects and merits of various complexes.

The remainder of present work is laid down as follows. In the next section, we explain the model system and present the simulation details. In section 3, the complexes composed of various kinds of polycations are investigated and discussed separately in the first part, and then a comparison regarding the physicochemical properties of those polyplexes follows. In the last section, a brief conclusion is given.

2. MODELING AND SIMULATION DETAILS

The model system is composed of a single DNA-like polyanion, numbers of polycations of a certain type, and plenty of monovalent counterions (positive and negative ones) that neutralize the entire system. The polyanion, as demonstrated in Figure 1a, is represented with a negatively charged linear chain
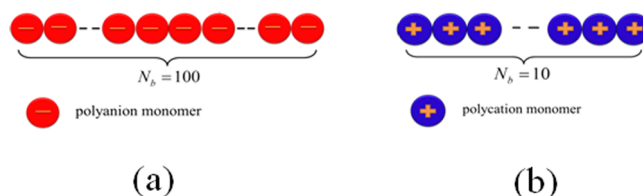

Figure 1. Schematic figure for homopolymers: (a) polyanion and (b) polycation. Each bead represents a monomer, and the number N_b in each figure represents the number of beads incorporated in the block. See text for details.

composed of 100 beads. Whereas the net charge on each base pair in a double-stranded DNA varies at different solvent environment,[42] we typically assign a unit negative charge on each bead of polyanion chain. In the present work, different types of polycations are considered including di- and triblock copolymers. i.e., the polycation is composed of a positively charged block and one or two neutral block(s). The neutral block is either hydrophobic or hydrophilic. By using the letters "P", "W", and "O" to represent the positively charged block, hydrophilic block (i.e., water-soluble), and hydrophobic block (i.e., oil-soluble), respectively, we abbreviate the type of a diblock copolymer with the combination of two corresponding letters, and the type of a triblock copolymer with the combination of three corresponding letters. Similarly, the complex formed with $\alpha\beta\eta$ polycations (α, β, η = P, W, O) is denoted as $\alpha\beta\eta$-polyplex. For example, PWO polymer represents a triblock polycation with a positively charged block at one end, a hydrophobic block at the other end, and a hydrophilic block in the middle. Correspondingly, the complex comprising the polyanion and PWO polycations is called PWO-polyplex.

The polycations under investigation mainly refer to two types of diblock copolymers, i.e., PO as shown in Figure 2a and
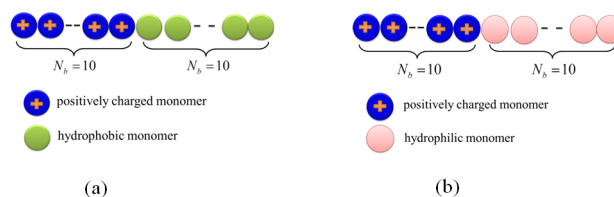

Figure 2. Same as Figure 1 but for diblock polycations: (a) PO polycation and (b) PW polycation.

PW in Figure 2b, and three types of triblock copolymers, i.e., POW, PWO, and WPO as shown in Figure 3a−c, respectively.
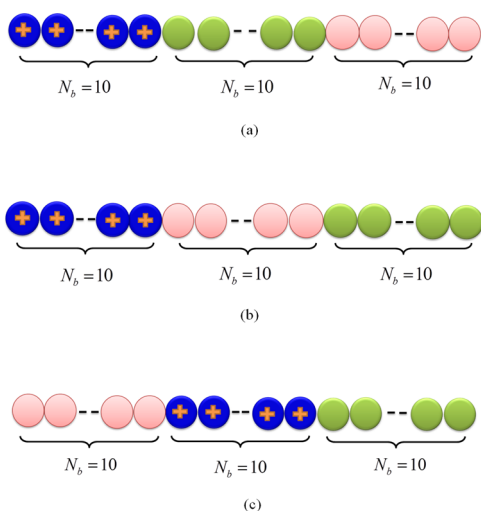

Figure 3. Same as Figure 2 but for triblock polycations: (a) POW-polycation, (b) PWO-polycation, and (c) WPO-polycation;. The representations of beads in colors are the same as those in Figure 2

All beads incorporated in the polymer chain, together with the monovalent counterions, are set with the same mass m and the same diameter σ. The solvent is treated as continuous medium with permittivity ξ. In our simulation, systems are described with energy unit ε, length unit σ, and mass unit m.

Both polycations and polyanion are described with bead−spring chains characterized with finitely extendable nonlinear elastic (FENE) potential[30,38,41]

$$u_{ij}^{\textbf{FENE}}(r) = \begin{cases} -\dfrac{1}{2}kR_0^2 \ln\left[1 - \left(\dfrac{r}{R_0}\right)^2\right] & r \leq R_0 \\ \infty & r > R_0 \end{cases} \tag{1}$$

Here, $k = 7\varepsilon/\sigma^2$ is the spring constant and $R_0 = 2\sigma$ is the maximum extension. With such assignment, the averaged bond length $\bar{r} = 1.1\sigma$. Those parameters are taken from Stevens's work where extensive simulations on DNA modeled with bead−spring chain were performed.[38,43] Regarding the nonbonding interaction, a truncated and shifted Lennard-Jones (LJ) potential is adopted to mimic the nonelectrostatic interactions among hydrophilic and hydrophobic beads, i.e., the short-range interaction between particles i and j with distance r follows

$$u_{ij}^{\textbf{LJ}}(r) = \begin{cases} 4\varepsilon\left[\left(\dfrac{\sigma}{r}\right)^{12} - \left(\dfrac{\sigma}{r}\right)^6 - \left(\dfrac{\sigma}{r_c}\right)^{12} + \left(\dfrac{\sigma}{r_c}\right)^6\right] & r < r_c \\ 0 & r \geq r_c \end{cases} \tag{2}$$

where r_c is the cutoff distance. As demonstrated in our previous work,[44] such simple model can effectively describe the hydrophilic and hydrophobic interactions by setting different cutoff values; i.e., a cutoff distance $r_c = 2.5\sigma$ is adopted to describe the attractive interaction between two hydrophobic beads, and the other cutoff value $r_c = 2^{1/6}\sigma$ can be introduced to describe the repulsive interaction of all other bead-pairs, i.e., the

pair containing a counterion, or a charged polymer bead or a neutral hydrophilic polymer bead. This simple model was developed basing on the idea that solvent-induced interaction between solutes, which can be characterized by potential of mean force,[45] depends on the local density of solvent in the surrounding area.[46] Particularly, when a solute is hydrophilic, it is surrounded tightly by water molecules, resulting in a purely repulsive potential to the other solute due to the excluded volume effect;[47] when both solutes are hydrophobic, the local solvent density in the vicinity of each solute is low, and a weak attraction between two solutes should be introduced.[38] To describe such solvent-induced potentials, the implicit Lennard-Jones models have been employed to investigate the behaviors of homopolymer chain in solvents with various solvent qualities.[48,49] We here extend the implicit Lennard-Jones models to describe the short-range interaction among hydrophilic/hydrophobic beads in the same solvent in addition to the long-range electrostatic interaction.

For the interaction between two charged beads, the Coulomb potential is additionally included. Such a long-ranged interaction is described with standard electrostatic potential; i.e., between the charged beads i and j with charge valence z_i and z_j, the Coulomb interaction follows

$$u_{ij}^{\text{ELE}}(r) = \frac{e^2}{4\pi\xi}\frac{z_i z_j}{r} = \frac{\lambda_B z_i z_j}{r}k_B T \tag{3}$$

where λ_B is Bjerrum length depending on the permittivity of the solvent via $\lambda_B = e^2/(4\pi\xi k_B T)$ with e being the charge unit, and $\xi = \xi_0 \xi_r$ with ξ_0 and ξ_r being the vacuum dielectric constant and the permittivity of solvent, respectively. k_B is Boltzmann constant, and T is the absolute temperature.

The interactions introduced above are all pairwise additive, i.e., supposing U_i is the total energy of bead i interacting with all the rest of the beads in the system, we have

$$U_i = \sum_{j \neq i}\left[u_{ij}^{\textbf{LJ}}(r) + u_{ij}^{\text{ELE}}(r) + u_{ij}^{\textbf{FENE}}(r)\right] \tag{4}$$

The simulation is performed at a constant temperature $T^* = k_B T/\varepsilon = 1.0$ and the motion of each bead is governed by Langevin equation

$$m\frac{d^2\mathbf{r}_i}{dt^2} = -\nabla U_i - \gamma\frac{d\mathbf{r}_i}{dt} + \mathbf{W}_i(t) \tag{5}$$

with the random force $W_i(t)$ satisfying $\langle W_i(t)W_i(t')\rangle = 6k_B T\gamma\delta_{ij}\delta(t - t')$. Here γ is the friction coefficient, and a moderate value of $\gamma = 1.0\tau^{-1}$ is chosen. The dynamical equation is solved with standard velocity verlet method[59] as detailed in the Supporting Information.

Since the Bjerrum length of water in the room temperature is 0.71 nm, we take λ_B as 0.71 nm all through this work. We set $\sigma = \lambda_B/2$ and Coulomb strength parameters $\Gamma = \lambda_B/\bar{r} = 1.8$ for representing strong polyelectrolyte.[38] Since the block length effect is beyond the research scope of current work, we simply set the block length as $N_b = 10$ for each block in polycation. The electrically neutral system is placed in a cubic box with box length $L = 100\sigma$, and periodic boundary condition is applied in all three dimensions. As checked in the Supporting Information, the simulation box is sufficiently large so that the finite size effect[50,60] is negligible. The electrostatic interactions are calculated with Particle Mesh Ewald (PME) algorithm.[51,52] The integral time step is set as 0.005τ with $\tau = \sigma(m/\varepsilon)^{1/2}$. The total time for each simulation is 8×10^6 steps,

and the equilibrium properties presented below are all obtained by taking ensemble average over the last 5×10^6 steps. The sufficiency of the simulation time for equilibration is validated by evaluating the square radius of gyration of polyanion every 5×10^3 steps, and no apparent variation of this quantity has been observed after around 2.5×10^6 steps.

The square radius of gyration of polyanion chain reflects the packing degree of polyanion chain in the complex,[36,37] and it is calculated by

$$\langle R_g^2 \rangle = \frac{1}{N^2} \sum_{i=1}^{N} \sum_{j=i}^{N} \langle (\mathbf{R}_j - \mathbf{R}_i)^2 \rangle \tag{6}$$

Here, $N = 100$ is the total number of monomers and R_i and R_j are the positions of monomers i and j in polyanion. The angular bracket in the above equation stands for ensemble average.

Radial distribution functions (RDFs) give detailed structural information on the polyplex. We calculate the RDFs, i.e., $g(r/\sigma)$, around polyanion for three types of beads: charged, hydrophilic, and hydrophobic neutral monomers. Each RDF is calculated by

$$g(r/\sigma) = \frac{n(r/\sigma)}{(4\pi/3)(r/\sigma)^3 \rho^0} \tag{7}$$

where $n(r/\sigma)$ is the statistically averaged number of monomer of a certain type at distance r/σ to a polycation bead, and ρ^0 is the corresponding monomer number density in the system. Besides the square radius of gyration and RDF, other structural properties including aggregation number, binding percentage, and zeta potential are also investigated as discussed below.

The effect of concentration of polycations on those physicochemical properties is considered. Similar to the conventional definition,[20,27,53] we adopt shorthand notations ρ_+ and ρ_- denoting the densities of positively charged monomer and negatively charged monomer. Because in each polymer chain the number of positively charged monomer or negatively charged one is fixed in the present study, ρ_+ and ρ_- reflect virtually the concentrations of polycation chain and polyanion chain. To state the relative concentration, we introduce Z to represents ρ_+/ρ_-. Apparently, when Z equals one, the polyplex is neutral; when Z is larger than one, the entire polyplex is positively charged; otherwise, it is negatively charged.

3. RESULTS AND DISCUSSION

3.1. Complexes of Different Polycations and Polyanion.
For the purpose of comparison, the polycationic homopolymer is first considered. Figure 4 depicts the adsorption process of P-polycations with the single polyanion
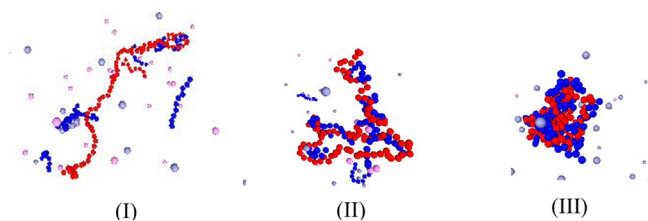

Figure 4. Three typical snapshots during the adsorption of polycationic homopolyers (P) onto the single polyanion chain at charge ratio $Z = 2$. The red chain represents polyanion, the blue chains stand for polycations, and the rest are counterions.

at a typical charge ratio $Z = 2$. At this ratio, the concentration of polycation chain is high enough to form globule-like polyplex. This ratio in simulation corresponds to a real concentration of polycation as $\rho_c = 0.742$ mmol/L. Three typical snapshots are displayed in Figure 4, and they represent three adsorption stages. Note that five parallel simulations with different initial coordinates and velocities are accessed, and similar conformations have been found in each adsorption stage. In the first stage, the positively charged beads of polycation approach onto the single polyanion due to the strong direct electrostatic attraction. In the second stage, the complex evolves from a loosened structure to a compact one. In the final stage, a stable complex with spherical-like globule is formed as depicted in Figure 4III. During this process, the electrostatic interaction dominates. Recently, Igor[13] investigated the formation of a complex with linear 13.4 kDa poly(ethylene imine) (LPEI) and plasmid DNA, and a similar phenomenon has been observed.

Next, we consider the systems composed of diblock polycations. Obviously, PW is a double hydrophilic diblock copolymer, and its binding process with the single polyanion is depicted in Figure 5A at charge ratio $Z = 2$. Such concentration
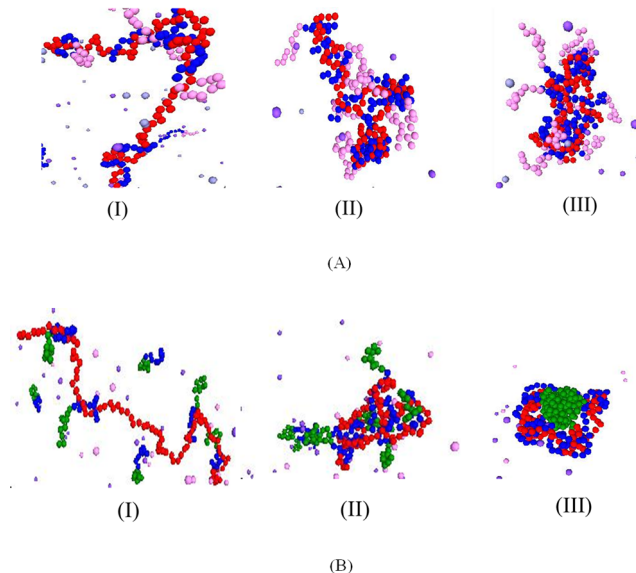

Figure 5. Adsorption processes of diblock polycations onto the polyanion at a charge ratio $Z = 2$ for (A) PW-polyplex and (B) PO-polyplex. Negatively charged beads in the polyanion are in red, and positively charged, hydrophobic, and hydrophilic neutral beads in the polycations are in blue, green, and pink, respectively. The rest are counterions.

is sufficiently high to form micelle around the single polyanion.[54,55] Similarly, the adsorption process can also be divided into three typical stages. It is noted that with the incorporation of a hydrophilic block, the chain length of each polycation becomes larger and thus polycation chains become more extendable in aqueous solvent due to its hydrophilicity, and this feature, as shown in Figure 5A, leads to the PW-polyplex with core−corona morphology. Different to PW-polyplex, PO-polyplex presents a tadpole-like morphology in aqueous solvent at the same polycation chain concentration. Specifically, the hydrophobic blocks are packed in the center of polyplex and surrounded by the charged blocks. Different to the formulation process of PW-polyplex, a self-assembly behavior associated with polycation is observed in the first stage of the
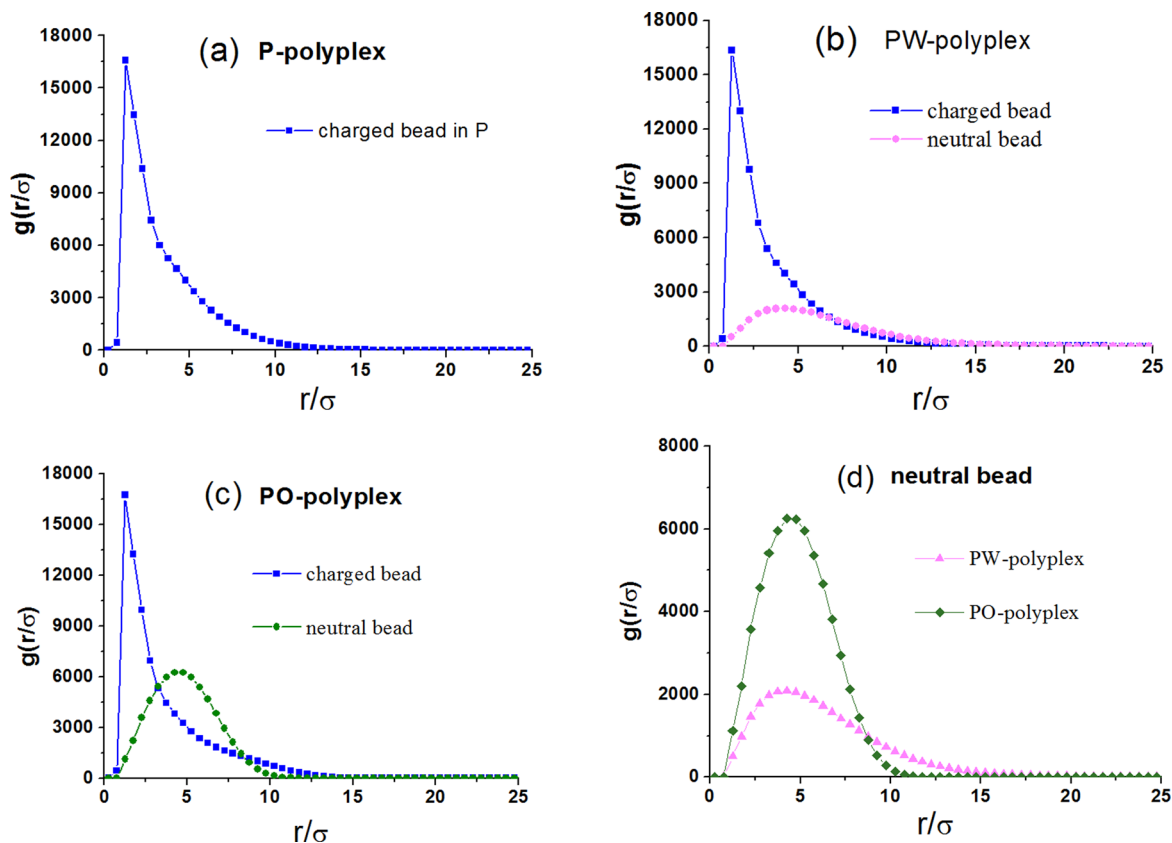
Figure 6. Radial distribution functions of different types of beads in the homo- and diblock polycations around the polyanion at fixed charge ratio Z = 2: (a−c) RDFs in three individual systems as self-described, and (d) comparison of RDFs for neutral bead around polyanion in different diblock-polycation based polyplexes.

PO-polyplex formation due to the attractive potential between pairs of hydrophobic beads within the same chain (see the green beads in Figure 5B(I)).

The internal morphology of the complex at equilibrium is studied by accessing the RDFs of various types of beads around the polyanion. Figure 6a−c presents the RDFs for charged and/or neutral bead(s) in complex around the polyanion at a fixed charge ratio Z = 2. It should be noted that, because the polyanion locates not necessarily at the center of polyplex, the RDFs in Figure 6 (and also in Figure 8) cannot reflect the actual layer structure of complex. Nevertheless, RDF reflects the averaged distance of other types of beads to polyanion. Figure 6 shows that there are no obvious differences for the RDF curves of charged bead around polyanion in three different polyplexes, and this is because the concentration of charged bead is low while the electronic attraction is very strong. Furthermore, we find that the peaks in those three RDF curves appear at the same distance around $r = 1.25\sigma$, and this confirms that the charged beads in polycations locate in the close vicinity of polyanion due to the strong Coulombic attraction. For neutral beads the RDFs in two diblock-polycation based polyplexes are very distinct. As shown in Figure 6d, the pink curve with triangles represents the RDF of hydrophilic bead around the polyanion in PW-polyplex, and the green curve with diamonds represents the RDF of hydrophobic bead in the vicinity of polyanion in PO-polyplex. Whereas the locations for the first peaks in both RDFs are almost the same, the peak heights are apparently different. The peak height of green curve is much higher than that of pink curve, and this confirms that hydrophobic block is assembled closely in

complex while the hydrophilic block extends freely into the aqueous solvent.

In general, the incorporation of hydrophobic block leads to a compact structure of the polyplex,[56] and the incorporation of hydrophilic block increases water-solubility of polyplex but reduces the polyanion stabilization.[20,23] It has been reported that the polycation can adsorb cationic serum proteins on the surface of the complex, while the cationic serum proteins were found to inhibit the transfection efficiency.[2] Whereas the hydrophilic modification of polycation can resist serum proteins due to the chain flexibility and electrical neutrality of hydrophilic block together with the absence of functional groups on the block, it usually results in a dissociation of polyplex prematurely under the physiological environment and thereafter leads to a degradation of DNA fragments by serum nucleases.[17] This defect is mainly caused by the strong hydrophilicity of polycation, which significantly weakens the binding affinity of the polycation to DNA.[17,25] In order to overcome the obstacles, many efforts have been attempted toward the delivery complexes formulated with multiblock polymers. Along this direction, a few ABC-type triblock copolymers have been engineered and evaluated,[17,25,26,57] and unfortunately, not all of them display much superior transfection efficiency.[17,27]

Three polyplexes, i.e., POW-polyplex, PWO-polyplex, and WPO-polyplex, are simulated. Figure 7 depicts the typical snapshots during the processes of complex formation involving three types of triblock polycations. At the first beginning, polycations in all systems extend in aqueous solvent with hydrophobic blocks self-aggregated. With more polycations
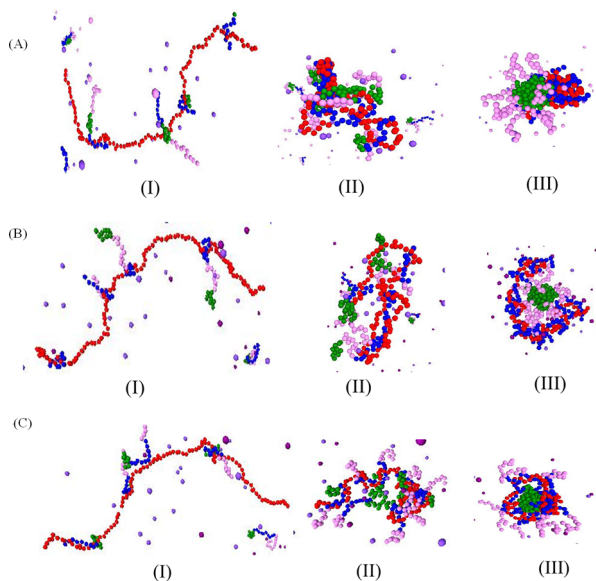
Figure 7. Adsorption processes of triblock polycations onto the polyanion at a charge ratio Z = 2 for (A) POW system, (B) PWO system, and (C) WPO system. The colors for the beads are the same as those in Figure 5.

approaching the single polyanion, the complex in each system evolves from a loose configuration to a core−corona structure. In particular, in POW- and WPO-polyplexes, hydrophilic blocks act as the corona-forming components stretching freely into aqueous solvent and hydrophobic blocks self-assemble. Polyanion beads wrap with the positively charged beads in polycations and form another aggregation, which finally forms the core surrounded by the neutral blocks. However, in PWO system, the hydrophilic blocks locate around the self-assembled

region of hydrophobic blocks, and the negatively charged polyanion chain and the positively charged blocks in polycation chains twist together due to the electrostatic attraction and wrap the neutral core. Such a difference in the morphology of polyplex is confirmed in Figure 8 in which the RDFs of various types of beads around the polyanion are plotted.

Figure 8 shows that, similar to the diblock-polycation based polyplex, the positively charged beads in triblock-polycation based polyplex is closely adsorbed on the polyanion. Combining Figures 7 and 8, we can find that in POW- and WPO-polyplexes the outer layers swing freely into the aqueous solvent, while in PWO system the peak location for the distribution of hydrophobic neutral beads moves outward significantly (see Figure 8d), and this indicates that the hydrophobic blocks in PWO-polyplex locate remote from the polyanion bead due to the steric hindrance stemmed from the presence of hydrophilic blocks. The combination of Figures 7 and 8 shows that for PWO systems the hydrophilic blocks lie in the outer layer and the hydrophobic blocks self-assemble forming the core. Besides, the oppositely charged beads twist together and surround the hydrophobic core leading to a loose structure. We further compare POW-polyplex and WPO-polyplex by checking the water-solubility. For WPO system plotted in Figure 8c, the peaks for the distributions of hydrophilic and hydrophobic neutral beads both locate at $r = 4.25\sigma$, and this is because the positively charged block locates in the middle of the triblock copolymer, and it is adsorbed onto polyanion dragging the neutral blocks at both ends of triblock copolymer. However, for POW system displayed in Figure 8a, the peaks of the distributions of hydrophobic and hydrophilic beads locate at different places, and in addition the peak for hydrophilic beads is more remote than that for hydrophobic beads, and this indicates that POW-polyplex is more water-soluble than WPO-polyplex.
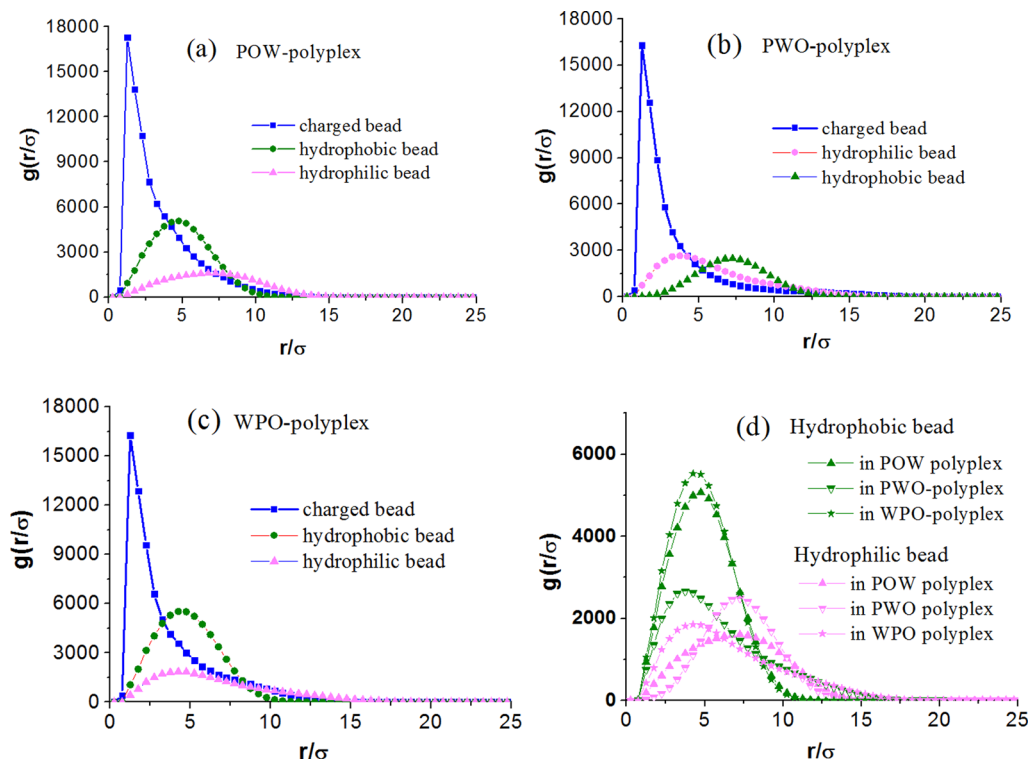

Figure 8. Same as Figure 6 but for triblock polycation systems.

3.2. Discussion and Comparison. To perform a quantitative comparison between di- and triblock based polyplexes, we further investigate the properties including the mean square radius of gyration of the polyanion. As explained above, the mean square radius of gyration reflects the packing degree of polyanion chain in the complex, and such packing degree can be measured in experiment by using fluorescence technique. The lower the intensity of fluorescence, the more tightly the polyanion is packed inside. Figure 9 plots the
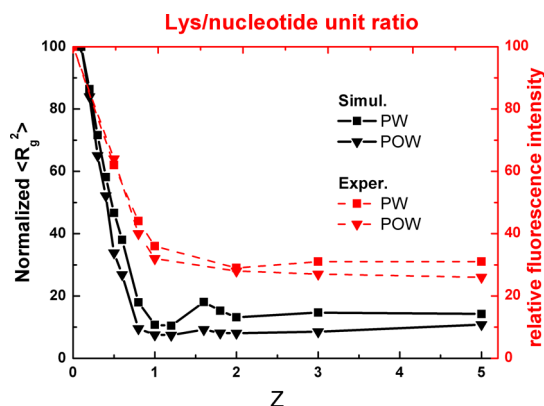

Figure 9. Normalized mean square radius of gyration in comparison with the relative fluorescence intensity from experiment.[27]

fluorescence intensity from Fukushima[27] (dashed red curves). In their experiment, the complex was formed with di- or triblock copolymers together with plasmid DNA (pDNA) in strong polyelectrolyte, and then characterized with an ethidium bromide (EtBr) exclusion assay. Particularly, the dashed curve with squares represents PEG-PLL (with 48 PLL units), which corresponds to PW-polycation in our simulation; the dashed curve with triangles stands for PEG-PMPA-PLL (with 36 PMPA units and 50 PLL units). Although the middle PMPA segment was used mainly for the purpose as endosomal buffering domain in experiment,[27] the amino groups of PMPA were deprotonated and uncharged in the solution of pH = 7.4 due to its low pK_a value (~ 6.2), and thus, it presents hydrophobic property and can be considered as a POW-polycation. The corresponding normalized mean square radii of gyrations from simulation for the polyanions in PW- and in POW-polyplexes are also plotted in Figure 9. The normalized mean square radius of gyration is obtained by linearly scaling the original value and setting the maximum value as 100. It is to be noted that in our simulation the charge valence in each charged bead is the same regardless of the sign, and thus, the Z value can be interpreted as the bead number ratio. Whereas a quantitative relation between the fluorescence intensity in experiment and the normalized mean square radius of gyration in simulation is yet to be built, a qualitative comparison can be made. Figure 9 shows that when $Z < 1$, the polyanion is packed more and more tightly with the increase of polycation concentration; While Z is large, the degrees of packing reach their individual plateaus. On this perspective, the simulation predictions agree well with the experimental observations. Besides, the experimental results showed that the POW-polyplex presented lower relative fluorescence intensity, or equivalently higher packing degree, than the PW-polyplex due to the hydrophobic modification of polycation. This feature is also faithfully predicted by our simulation, which coincides with another recent experiment observation by Sharma.[17] Sharma

incorporated a hydrophobic middle block into the conventional PEG-polycation architecture and found the resulting POW-polyplex provided better protection of DNA from enzymatic degradation.[17]

Figure 10 plots the mean square radii of gyrations of polyanion chains for different polyplexes as a function of Z. It
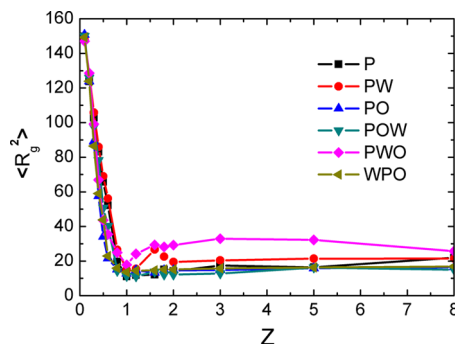

Figure 10. Mean square radius of gyration of the polyanion in polyplex versus concentration ratio Z.

shows that in terms of packing degree, among triblock copolymers the POW polycation has slightly better performance than WPO polycation and much better performance than PWO polycation. While among diblock copolymers, the PO polycation is prior to the PW polycation. When comparing the performances between the triblock copolymer and the diblock copolymer, we notice that a hydrophobic modification of PW polycation will not necessarily lead to a better performance on packing degree, and the modification at different locations in polycationic chain may lead to very different results, e.g., while POW-polycation based polyplex provides better packing effect of polyanion than PW-polycation based polyplex, which is consistent with the observation reported by Sharma et al.,[17] the PWO-polycation based polyplex has worse packing effect.

To gain further understanding about the effects of concentration on the complex structure, we compute the number of beads aggregated around the single polyanion. The aggregation is accounted when a bead in polycationic chain is located within the distance of r_p around a polycation bead, and here, r_p is the location of the remote peak in RDFs displayed in Figure 6 or 8. The aggregation number reflects the packing degree of the polyplex. Figure 11 plots the aggregation number in P-polyplex comparing those in PO- and PW-polyplex at different values of Z. It can be found that when $Z < 1$, the
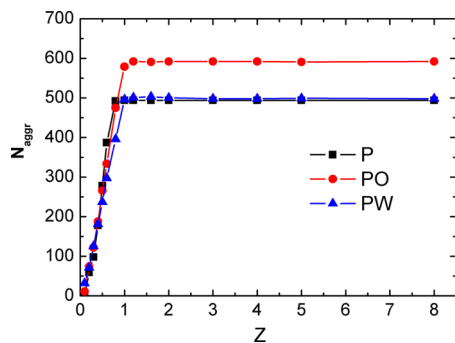

Figure 11. Distribution of aggregation number around polyanion as a function of Z in the polyplex formed with homo- or diblock polycation.

aggregation numbers in the three polyplexes increase linearly with Z, and this is because in this range the concentration of polycation is still below the saturation value in the vicinity of polyanion, and then as a consequence the aggregation number increases with the concentration of polycation. However, after Z reaching a threshold value, i.e., $Z = 1$ corresponding to the electronic neutrality of polyplex, the aggregation numbers become nearly constant. This shows when Z further increases, the additionally introduced polycations can be no longer adsorbed onto the polyplex due to the electronic repulsion, and this phenomenon is also observed in the simulation process. In particular, Figure 11 shows that the plateau of the curve for PO-polyplex is higher than those for two other polyplexes, and this indicates that the PO-polyplex has more compact structure than P-polyplex and PW-polyplex. In the present work, the strengths of hydrophobicity and hydrophilicity are fixed by specifying the energy parameter $\varepsilon = k_BT$ in the truncated and shifted LJ, and such value presents a strong hydrophobic attraction. In experiment, the strength of hydrophobicity varies in different sample systems. Generally, the aggregation number is larger when the hydrophobic attraction is stronger, and vice versa.

The aggregation numbers for the polyplexes formed with various triblock polycations are also calculated and compared in Figure 12. Generally, triblock-polycation based polyplex present
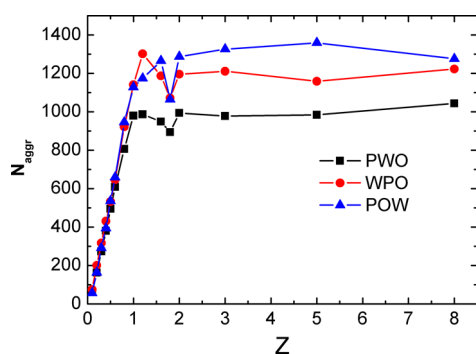

Figure 12. Distributions of aggregation number as a function of Z for triblock-polycation based polyplexes.

higher aggregation number than diblock-polycation based polyplex. When $Z < 1$, similar trend as in diblock-polycation based polyplex is observed, i.e., the aggregation numbers increase linearly with the polycation concentration; when Z is larger than one, the aggregation numbers in three polyplexes reach their individual plateaus, and in addition, one can notice that in terms of the magnitudes of those plateaus we have POW > WPO > PWO, and this shows that the POW-polyplex presents the highest packing degree. This trend is consistent with Figure 7. Surprisingly, different to the case of diblock polycation based polyplex, the distributions of aggregation number have an apparent jump at around $Z = 1.8$ in three triblock-polycation based polyplexes. This is likely because a small size variation of the polyplex occurs at this concentration ratio.

In order to investigate the amount of polycation beads bound onto the polyanion chain, we calculate the binding percentage. The binding percentage is defined as the ratio of polycation bead number to its corresponding value at $Z = 1$ in the present work. Figure 13 plots the binding percentages from our simulation (black solid curves) for P-polyplex and PO-polyplex. For comparison, we also plot the binding percentages from
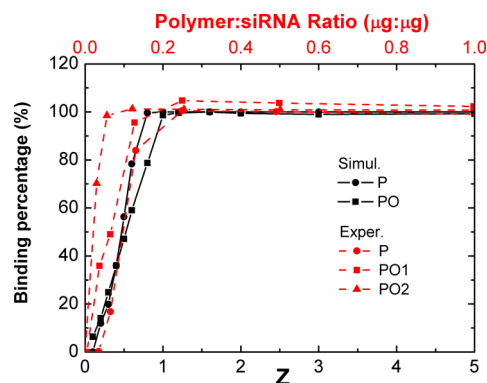

Figure 13. Comparison of binding percentage from simulation (as a function of Z) and from experiment (in mass ratio of polymer and siRNA). For experimental curves, P refers to PEI, and PO1 and PO2 refer to PEI-StA1 and PEI-StA2 in ref 58, respectively.

experiment (red dashed curves) determined using gel migration assay associated with densitometry.[58] In the experiment the binding percentage is related to the mass ratio of polymer to siRNA, and such mass ratio can be in principle converted into the ratio of polycation bead number to siRNA bead number (or equivalently Z) given the types of both polymer and siRNA were specified. In other words, the definition of binding percentage in experiment is different from but essentially equivalent to the definition given here. Nevertheless, due to the lack of knowledge on the degree of protonated amines in the experiment, the N/P ratio cannot be qualitatively determined from the mass ratio. For this reason the comparison is displayed with double x-coordinates. The comparison shows that the simulation predictions agree qualitatively well with the experiment measurements. Besides, the binding percentage quickly reaches a plateau for each polyplex when Z exceeds one. Indeed, when $Z > 1$, the binding percentage is slightly greater than 100% indicating that the diblock-polycation based polyplex is a little positively charged. Attention should be paid to the polymers utilized in the experiment[58] that are branched with PEIs, and we consider those branches are generally short, and thus those polymers can be regarded as linear polycations in a coarse-grained manner and hereby are suitable for the comparison with our model system.

Finally, zeta potential is analyzed. Whereas low positive zeta potential on polyplex is helpful for gene delivery crossing cell membranes, it has been reported that polyplex with high positive zeta potential can adsorb serum and therefore reduce the transfection efficiency.[26] In our simulation the zeta potential is calculated by accounting the net charge of polyplex. Because the charge valence in each block is fixed, zeta potential is essentially proportional to the binding percentage, and both quantities reflect the binding degree of polycations to polyanion. Figure 14 plots the zeta potential for different di- and triblock polyplexes as a function of Z. The calculated zeta potentials are compared with experimental data, which was plotted in terms of N/P ratio.[17] It is shown that the simulation results generally agree well with the experimental observations. We notice that the POW polyplex presents higher zeta potential compared to PW polyplex when Z is large, and such a difference seems to originate from the presence of the additional hydrophobic block in POW polycation. We deduce that the attraction between a pair of hydrophobic beads can lead the polyplex to further adsorb polycationic chains after $Z = 1$, and this eventually causes the polyplex to become positively
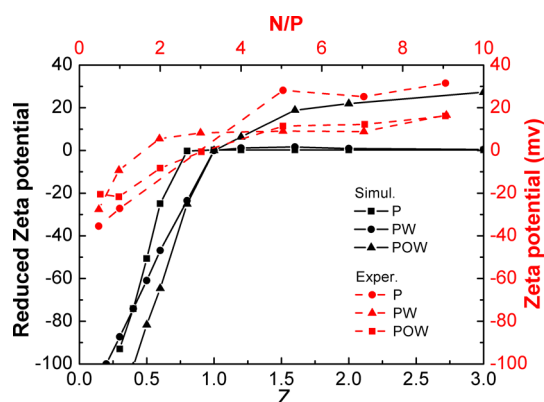
Figure 14. Zeta potentials for different di- and triblock polyplexes as a function of Z. Here P refers to PDMAEMA, PW refers to PEG-PDMAEMA, and POW refers to PEG-PnBA-PDMAEMA in the experiment.[17]

charged. To reduce the zeta potential of POW-polyplex, a weak hydrophobic block, for example, PMPA block,[27] can be adopted.

4. CONCLUSIONS

The present work reports a coarse-grained simulation study on the roles of neutral block in polycation/DNA-like complexes. With the help of an implicit solvent model involving simple expressions for hydrophobic and hydrophilic interactions, we investigate the morphology of polyplex, RDFs, aggregation number, mean square radius of gyration, binding percentage, etc., and the simulation results generally show qualitatively agreements with available experimental data. By comparing the physicochemical properties of those polyplexes composed of different diblock and triblock polycations, the conclusions can be drawn as follows:

First of all, a further hydrophobic/hydrophilic modification of diblock polycation does not necessarily lead to a better feature, and the effect of modification sensitively depends on the location of neutral block. Particularly, POW-polyplex offers an enhancement on the packing degree over PO- and PW-polyplex, which is consistent with the literature,[27] but the PWO-polyplex presents lower packing degree than diblock-polycation based polyplex; Second, based on the physicochemical properties, POW-polycation is beyond PWO-polycation and WPO-polycation as a gene carrier candidate. Indeed, POW-polyplex presents high packing degree and good water solubility, while WPO-polyplex is less water-soluble, and especially in PWO-polyplex the DNA-like polyanion is nearly naked and not protected in the solvent. Finally, the POW-polyplex presents a high zeta potential when the concentration of polycation chain is large, which may give rise to low transfection efficiency as discussed in experimental work.[17] We deduce the high zeta potential is due to the presence of hydrophobic segment and can be adjusted by tailoring the block length of such segment. Empirical evidence for this point is not yet available.

Generally, the hydrophobic/hydrophilic modifications of linear polycations may bring an improvement of one aspect of the properties as gene carrier but also will involve a trade-off with another one. However, we should emphasize that this general conclusion is reached upon the simulations involving only one linear polycation, and the behaviors for other kinds of polycations, e.g., dendrimer-like polymers, may be quite different. In addition, the interactions among polyanion chains could bring additional effects on the formation of polyplex. These are challenging problems but represent possible future direction of this work.

◼ ASSOCIATED CONTENT

ⓈSupporting Information

Simulation details and the discussion on finite size effect. The Supporting Information is available free of charge on the ACS Publications website at DOI: 10.1021/mp500861c.

◼ AUTHOR INFORMATION

Corresponding Authors
*E-mail: szhao@ecust.edu.cn.
*E-mail: xhan@ecust.edu.cn.

Notes
The authors declare no competing financial interest.

◼ ACKNOWLEDGMENTS

◼ REFERENCES

(1) Merdan, T.; Kopecek, J.; Kissel, T. Prospects for cationic polymers in gene and oligonucleotide therapy against cancer. *Adv. Drug Delivery Rev.* **2002**, *54* (5), 715−58.

(2) Han, S.-o.; Mahato, R. I.; Sung, Y. K.; Kim, S. W. Development of biomaterials for gene therapy. *Mol. Ther.* **2000**, *2* (4), 302−317.

(3) Godbey, W. T.; Mikos, A. G. Recent progress in gene delivery using non-viral transfer complexes. *J. Controlled Release* **2001**, *72* (1−3), 115−125.

(4) Lungwitz, U.; Breunig, M.; Blunk, T.; Göpferich, A. Polyethylenimine-based non-viral gene delivery systems. *Eur. J. Pharm. Biopharm.* **2005**, *60* (2), 247−266.

(5) Zhang, X.; Godbey, W. T. Viral vectors for gene delivery in tissue engineering. *Adv. Drug Delivery Rev.* **2006**, *58* (4), 515−534.

(6) Galanis, E.; Russell, S. Cancer gene therapy clinical trials: lessons for the future. *Br J. Cancer.* **2001**, *85* (10), 1432−1436.

(7) Anderson, W. Prospects for human gene therapy. *Science* **1984**, *226* (4673), 401−409.

(8) Ehtezazi, T.; Rungsardthong, U.; Stolnik, S. Thermodynamic analysis of polycation−DNA interaction applying titration micro-calorimetry. *Langmuir* **2003**, *19* (22), 9387−9394.

(9) Gebhart, C. L.; Sriadibhatla, S.; Vinogradov, S.; Lemieux, P.; Alakhov, V.; Kabanov, A. V. Design and formulation of polyplexes based on pluronic-polyethyleneimine conjugates for gene transfer. *Bioconjugate Chem.* **2002**, *13* (5), 937−944.

(10) McTaggart, S.; Al-Rubeai, M. Retroviral vectors for human gene delivery. *Biotechnol Adv.* **2002**, *20* (1), 1−31.

(11) Smith, A. E. Viral vectors in gene therapy. *Annu. Rev. Microbiol.* **1995**, *49* (1), 807−838.

(12) Akhtar, S.; Hughes, M. D.; Khan, A.; Bibby, M.; Hussain, M.; Nawaz, Q.; Double, J.; Sayyed, P. The delivery of antisense therapeutics. *Adv. Drug Delivery Rev.* **2000**, *44* (1), 3−21.

(13) Perevyazko, I. Y.; Bauer, M.; Pavlov, G. M.; Hoeppener, S.; Schubert, S.; Fischer, D.; Schubert, U. S. Polyelectrolyte complexes of DNA and linear PEI: formation, composition and properties. *Langmuir* **2012**, *28* (46), 16167−16176.

(14) Godbey, W. T.; Wu, K. K.; Mikos, A. G. Poly(ethylenimine) and its role in gene delivery. *J. Controlled Release* **1999**, *60* (2−3), 149−160.

(15) Boussif, O.; Delair, T.; Brua, C.; Veron, L.; Pavirani, A.; Kolbe, H. V. J. Synthesis of polyallylamine derivatives and their use as gene transfer vectors in vitro. *Bioconjugate Chem.* **1999**, *10* (5), 877−883.

(16) Haensler, J.; Szoka, F. C. Polyamidoamine cascade polymers mediate efficient transfection of cells in culture. *Bioconjugate Chem.* **1993**, *4* (5), 372−379.

(17) Sharma, R.; Lee, J.-S.; Bettencourt, R. C.; Xiao, C.; Konieczny, S. F.; Won, Y.-Y. Effects of the incorporation of a hydrophobic middle block into a PEG−polycation diblock copolymer on the physicochemical and cell interaction properties of the polymer−DNA complexes. *Biomacromolecules* **2008**, *9* (11), 3294−3307.

(18) Arigita, C.; Zuidam, N.; Crommelin, D. A.; Hennink, W. Association and dissociation characteristics of polymer/DNA complexes used for gene delivery. *Pharm. Res.* **1999**, *16* (10), 1534−1541.

(19) Luten, J.; van Nostrum, C. F.; De Smedt, S. C.; Hennink, W. E. Biodegradable polymers as non-viral carriers for plasmid DNA delivery. *J. Controlled Release* **2008**, *126* (2), 97−110.

(20) Petersen, H.; Fechner, P. M.; Martin, A. L.; Kunath, K.; Stolnik, S.; Roberts, C. J.; Fischer, D.; Davies, M. C.; Kissel, T. Polyethylenimine-graft-poly(ethylene glycol) copolymers: influence of copolymer block structure on DNA complexation and biological activities as gene delivery system. *Bioconjugate Chem.* **2002**, *13* (4), 845−854.

(21) Ahn, C.-H.; Chae, S. Y.; Bae, Y. H.; Kim, S. W. Biodegradable poly(ethylenimine) for plasmid DNA delivery. *J. Controlled Release* **2002**, *80* (1−3), 273−282.

(22) Ahn, C.-H.; Chae, S. Y.; Bae, Y. H.; Kim, S. W. Synthesis of biodegradable multi-block copolymers of poly(l-lysine) and poly-(ethylene glycol) as a non-viral gene carrier. *J. Controlled Release* **2004**, *97* (3), 567−574.

(23) Bronich, T.; Kabanov, A. V.; Marky, L. A. A thermodynamic characterization of the interaction of a cationic copolymer with DNA. *J. Phys. Chem. B* **2001**, *105* (25), 6042−6050.

(24) Hamley, I. W. PEG−peptide conjugates. *Biomacromolecules* **2014**, *15* (5), 1543−1559.

(25) Oishi, M.; Kataoka, K.; Nagasaki, Y. pH-responsive three-layered PEGylated polyplex micelle based on a lactosylated ABC triblock copolymer as a targetable and endosome-disruptive nonviral gene vector. *Bioconjugate Chem.* **2006**, *17* (3), 677−688.

(26) Miyata, K.; Oba, M.; Kano, M.; Fukushima, S.; Vachutinsky, Y.; Han, M.; Koyama, H.; Miyazono, K.; Nishiyama, N.; Kataoka, K. Polyplex Micelles from Triblock copolymers composed of tandemly aligned segments with biocompatible, endosomal escaping, and DNA-condensing functions for systemic gene delivery to pancreatic tumor tissue. *Pharm. Res.* **2008**, *25* (12), 2924−2936.

(27) Fukushima, S.; Miyata, K.; Nishiyama, N.; Kanayama, N.; Yamasaki, Y.; Kataoka, K. PEGylated polyplex micelles from triblock catiomers with spatially ordered layering of condensed pDNA and buffering units for enhanced intracellular gene delivery. *J. Am. Chem. Soc.* **2005**, *127* (9), 2810−2811.

(28) Ziebarth, J.; Wang, Y. Molecular dynamics simulations of DNA-polycation complex formation. *Biophys. J.* **2009**, *97* (7), 1971−1983.

(29) Elder, R. M.; Jayaraman, A. Coarse-grained simulation studies of effects of polycation architecture on structure of the polycation and polycation−polyanion complexes. *Macromolecules* **2012**, *45* (19), 8083−8096.

(30) Stevens, M. J.; Plimpton, S. J. The effect of added salt on polyelectrolyte structure. *Eur. Phys. J. B* **1998**, *2* (3), 341−345.

(31) Sun, C.; Tang, T.; Uludağ, H.; Cuervo, J. E. Molecular dynamics simulations of DNA/PEI complexes: effect of PEI branching and protonation state. *Biophys. J.* **2011**, *100* (11), 2754−2763.

(32) Hayashi, Y.; Ullner, M.; Linse, P. Oppositely charged polyelectrolytes. complex formation and effects of chain asymmetry. *J. Phys. Chem. B* **2004**, *108* (39), 15266−15277.

(33) Sun, C.; Tang, T. Study on the role of polyethylenimine as gene delivery carrier using molecular dynamics simulations. *J. Adhes. Sci. Technol.* **2012**, *28* (3−4), 399−416.

(34) Elder, R. M.; Emrick, T.; Jayaraman, A. Understanding the effect of polylysine architecture on DNA binding using molecular dynamics simulations. *Biomacromolecules* **2011**, *12* (11), 3870−3879.

(35) Maiti, P. K.; Bagchi, B. Structure and dynamics of DNA−dendrimer complexation: role of counterions, water, and base pair sequence. *Nano Lett.* **2006**, *6* (11), 2478−2485.

(36) Winkler, R. G.; Steinhauser, M. O.; Reineker, P. Complex formation in systems of oppositely charged polyelectrolytes: A molecular dynamics simulation study. *Phys. Rev. E* **2002**, *66* (2), 021802.

(37) Ziebarth, J.; Wang, Y. Coarse-grained molecular dynamics simulations of DNA condensation by block copolymer and formation of core−corona structures. *J. Phys. Chem. B* **2010**, *114* (19), 6225−6232.

(38) Stevens, M. J. Simple simulations of DNA condensation. *Biophys. J.* **2001**, *80* (1), 130−139.

(39) Hoda, N.; Larson, R. G. Explicit- and implicit-solvent molecular dynamics simulations of complex formation between polycations and polyanions. *Macromolecules* **2009**, *42* (22), 8851−8863.

(40) Jorge, A. F.; Dias, R. S.; Pais, A. A. C. C. Enhanced condensation and facilitated release of DNA using mixed cationic agents: a combined experimental and Monte Carlo Study. *Biomacromolecules* **2012**, *13* (10), 3151−3161.

(41) Crozier, P. S.; Stevens, M. J. Simulations of single grafted polyelectrolyte chains: ssDNA and dsDNA. *J. Chem. Phys.* **2003**, *118* (8), 3855−3860.

(42) Wu, J.; Zhao, S.-L.; Gao, L.; Wu, J.; Gao, D. Sorting short fragments of single-stranded DNA with an evolving electric double layer. *J. Phys. Chem. B* **2013**, *117* (8), 2267−2272.

(43) Stevens, M. J.; Kremer, K. The nature of flexible linear polyelectrolytes in salt free solution: A molecular dynamics study. *J. Chem. Phys.* **1995**, *103* (4), 1669−1690.

(44) Liu, Z.; Shang, Y.; Feng, J.; Peng, C.; Liu, H.; Hu, Y. Effect of hydrophilicity or hydrophobicity of polyelectrolyte on the interaction between polyelectrolyte and surfactants: molecular dynamics simulations. *J. Phys. Chem. B* **2012**, *116* (18), 5516−5526.

(45) Widom, B.; Bhimalapuram, P.; Koga, K. The hydrophobic effect. *Phys. Chem. Chem. Phys.* **2003**, *5* (15), 3085−3093.

(46) Kovalenko A. Three-dimentsional Rism theory for molecular liquids and solid-liquid interfaces. In *Molecular Theory of Solvation*; Hirata F., Ed.; Understanding Chemical Reactivity; Springer: New York, 2003; Vol. 24, pp 169−275.

(47) Rabani, E.; Egorov, S. A. Solvophobic and solvophilic effects on the potential of mean force between two nanoparticles in binary mixtures. *Nano Lett.* **2002**, *2* (1), 69−72.

(48) Seidel, C.; Netz, R. R. Individual polymer paths and end-point stretching in polymer brushes. *Macromolecules* **2000**, *33* (2), 634−640.

(49) Reddy, G.; Yethiraj, A. Solvent effects in polyelectrolyte adsorption: Computer simulations with explicit and implicit solvent. *J. Chem. Phys.* **2010**, *132* (7), 074903.

(50) Salacuse, J. J.; Denton, A. R.; Egelstaff, P. A. Finite-size effects in molecular dynamics simulations: Static structure factor and compressibility. I. Theoretical method. *Phys. Rev. E* **1996**, *53* (3), 2382−2389.

(51) Darden, T.; Perera, L.; Li, L.; Pedersen, L. New tricks for modelers from the crystallography toolkit: the particle mesh Ewald algorithm and its use in nucleic acid simulations. *Structure* **1999**, *7* (3), R55−R60.

(52) Darden, T.; York, D.; Pedersen, L. Particle mesh Ewald: An N·log(N) method for Ewald sums in large systems. *J. Chem. Phys.* **1993**, *98* (12), 10089−10092.

(53) Alvarez-Lorenzo, C.; Barreiro-Iglesias, R.; Concheiro, A.; Iourtchenko, L.; Alakhov, V.; Bromberg, L.; Temchenko, M.; Deshmukh, S.; Hatton, T. A. Biophysical characterization of complexation of DNA with block copolymers of poly(2-dimethylaminoethyl) methacrylate, poly(ethylene oxide), and poly(propylene oxide). *Langmuir* **2005**, *21* (11), 5142−5148.

(54) Han, S.-o.; Mahato, R. I.; Sung, Y. K.; Kim, S. W. Development of biomaterials for gene therapy. *Mol. Ther.* **2000**, *2* (4), 302−317.

(55) Kircheis, R.; Schüller, S.; Brunner, S.; Ogris, M.; Heider, K.-H.; Zauner, W.; Wagner, E. Polycation-based DNA complexes for tumor-targeted gene delivery in vivo. *J. Gene Med.* **1999**, *1* (2), 111−120.

(56) Liu, Z.; Zhang, Z.; Zhou, C.; Jiao, Y. Hydrophobic modifications of cationic polymers for gene delivery. *Prog. Polym. Sci.* **2010**, *35* (9), 1144−1162.

(57) Patil, M. L.; Zhang, M.; Minko, T. Multifunctional triblock nanocarrier (PAMAM-PEG-PLL) for the efficient intracellular siRNA delivery and gene silencing. *ACS Nano* **2011**, *5* (3), 1877−1887.

(58) Alshamsan, A.; Haddadi, A.; Incani, V.; Samuel, J.; Lavasanifar, A.; Uludağ, H. Formulation and delivery of siRNA by oleic acid and stearic acid modified polyethylenimine. *Mol. Pharm.* **2008**, *6* (1), 121−133.

(59) Rapaport, D. C. *The Art of Molecular Dynamics Simulation*, 2nd revised ed.; Cambridge University Press; Cambridge, U.K., 2004; pp 18−19.

(60) Fraga, E. S.; Venugopalan, R. Finite-size effects on nucleation in a first-order phase transition. *Cem. Concr. Res.* **2009**, *39* (10), 849−860.

K